CORE
Metadata, citation and similar papers at core.ac.uk
Provided by Infoscience - École polytechnique fédérale de Lausanne

Journal of Neurochemistry
Lippincott–Raven Publishers, Philadelphia
© 1998 International Society for Neurochemistry

Steady-State Cerebral Glucose Concentrations and Transport in the Human Brain

*Rolf Gruetter, *†‡Kâmil Ugurbil, and †Elizabeth R. Seaquist

*Departments of *Radiology, †Medicine, and ‡Biochemistry, Center for MR Research and Clinical Research Center, University of Minnesota, Minneapolis, Minnesota, U.S.A.*

Abstract: Understanding the mechanism of brain glucose transport across the blood–brain barrier is of importance to understanding brain energy metabolism. The specific kinetics of glucose transport have been generally described using standard Michaelis–Menten kinetics. These models predict that the steady-state glucose concentration approaches an upper limit in the human brain when the plasma glucose level is well above the Michaelis–Menten constant for half-maximal transport, K_t. In experiments where steady-state plasma glucose content was varied from 4 to 30 m*M*, the brain glucose level was a linear function of plasma glucose concentration. At plasma concentrations nearing 30 m*M*, the brain glucose level approached 9 m*M*, which was significantly higher than predicted from the previously reported K_t of ~4 m*M* ($p < 0.05$). The high brain glucose concentration measured in the human brain suggests that ablumenal brain glucose may compete with lumenal glucose for transport. We developed a model based on a reversible Michaelis–Menten kinetic formulation of unidirectional transport rates. Fitting this model to brain glucose level as a function of plasma glucose level gave a substantially lower K_t of 0.6 ± 2.0 m*M*, which was consistent with the previously reported millimolar K_m of GLUT-1 in erythrocyte model systems. Previously reported and reanalyzed quantification provided consistent kinetic parameters. We conclude that cerebral glucose transport is most consistently described when using reversible Michaelis–Menten kinetics. **Key Words:** NMR—Glucose transport—In vivo studies—Spectroscopy—Human.
J. Neurochem. **70,** 397–408 (1998).

Knowledge of the specific mechanism of glucose transport across the blood–brain barrier is important for understanding cerebral carbohydrate metabolism, which is the major source of energy for ATP production. Glucose transport across the blood–brain barrier occurs by facilitated diffusion mediated by specific transporter proteins. Glucose extraction is a saturable process in the brain (Crone, 1965) and erythrocytes (Le Fevre, 1961) and is mediated by facilitated diffusion that has been well-established to be stereospecific and substrate-specific. Standard Michaelis–Menten models for glucose transport kinetics have since been used almost exclusively in most studies of the brain (for reviews, see, e.g., Lund-Andersen, 1979; Pardridge, 1983; Gjedde, 1992), with one exception (Cunningham et al., 1986).

Many elegant techniques have been applied to study brain glucose uptake. The indicator-dilution techniques sample tracer extraction with a single pass across the capillary bed at a very high time resolution but with a somewhat limited spatial resolution (Knudsen et al., 1990). On the other hand, state-of-the art tracer techniques, such as positron emission tomography (PET), can provide a high spatial resolution (Svarer et al., 1996). However, the information on cerebral glucose content is indirect because the active metabolism of labeled glucose implies substantial label accumulation in metabolic products that cannot be distinguished from native glucose. To overcome this limitation, glucose analogues that are not metabolized, such as methylglucose, have also been used (Brooks et al., 1986; Feinendegen et al., 1986). Unfortunately, using glucose analogues has the disadvantage that the physical and apparent distribution volumes of the analogue may not be identical to those of D-glucose. It has therefore become customary to relate the measurements to native glucose by using suitable conversion constants such as the lumped constant, which itself depends on precise knowledge of tissue glucose content (Reivich et al., 1985). Cerebral glucose content is dictated by the transport capacity of the blood–brain barrier as well as the metabolic consumption.

Glucose transport across membranes is mediated by a family of transporter proteins (Mueckler, 1994). The majority of evidence has suggested that the ubiquitous high-affinity transporter present in erythrocyte mem-

Received May 13, 1997; revised manuscript received August 15, 1997; accepted August 18, 1997.
Address correspondence and reprint requests to Dr. R. Gruetter at Center for MR Research and Clinical Research Center, 385 East River Road, Minneapolis, MN 55455, U.S.A.

Abbreviations used: CBV, cerebral blood volume; CMR, cerebral metabolic rate; Cr, creatine; MR, magnetic resonance; MRI, magnetic resonance imaging; MRS, magnetic resonance spectroscopy; PET, positron emission tomography; ppm, parts per million.

branes, GLUT-1, is also the dominant transporter protein at the blood–brain barrier, with minor contributions from other transporters (Kalaria et al., 1988; Gerhart et al., 1992; Maher et al., 1993). Inside the brain, a different transporter may be responsible for glucose transport across the cell membranes. However, several studies have suggested that the large surface area of brain cells may result in rapid equilibration inside the brain's aqueous phase leading to similar intra- and extracellular glucose concentrations (Lund-Andersen, 1979; Gjedde and Diemer, 1983; Holden et al., 1991; Gjedde, 1992; Silver and Erecińska, 1994; Whitesell et al., 1995).

Because the transporter isoform at the blood–brain barrier and that at the erythrocyte membrane are very similar, the kinetic constant for half-maximal transport, K_t, should in principle be of similar magnitude. However, when reviewing the literature on animal brain glucose transport, a noticeable distribution of the measured brain K_t was observed, ranging from 2 to 14 mM, as previously reviewed (Gjedde, 1992; Mason et al., 1992). Likewise, the reported K_m for glucose transport varies in the erythrocyte from 0.5 mM in the zero-trans entry experiments to the equilibrium exchange K_m of 30 mM (Carruthers, 1990). Noteworthy is the observation that in the studies in the erythrocyte, which is a system of high purity and great simplicity, the Michaelis–Menten constants also appear to diverge substantially. Some of the discrepancy has been attributed to methodological inadequacies, and some may potentially be explained by differences in species-specific expression of GLUT-1 (Cloherty et al., 1996).

Localized glucose transport kinetic measurements in human brain (Brooks et al., 1986; Feinendegen et al., 1986; Blomqvist et al., 1991; Gruetter et al., 1992*a*, 1996*c*) have so far been highly consistent, with a Michaelis–Menten constant K_t of 4–5 mM for transport and an average maximal transport rate, T_{max}, of ~1 μmol/g/min (for reviews, see Gjedde, 1992; Gruetter et al., 1996*c*). These kinetic constants of the standard Michaelis–Menten model predicted that brain glucose content should be <5 μmol/g when plasma glucose content is <30 mM. However, the highest plasma glucose value previously examined was 13.5 mM, where any potential discrepancy of the model may have been masked by experimental scatter. The purpose of the present study was to confirm the predicted relationship between plasma and brain glucose at very high plasma glucose concentrations. A preliminary report has appeared (Gruetter et al., 1996*d*).

MATERIALS AND METHODS

Subjects

Eighteen healthy human subjects were studied in 23 studies after giving informed consent according to procedures approved by the Institutional Review Board: Human Subjects Committee. At the time of study, the subjects were 41 ± 13 years in age and weighed 67 ± 11 kg. On the morning of study, subjects reported to the Center for Magnetic Resonance Research after fasting overnight. In preparation for the clamp procedure, an intravenous catheter was placed antegrade in each forearm and retrograde in a foot. Extremities were warmed by placing preheated pads and water-soaked towels around the lower extremities. Somatostatin was infused into one arm vein at a progressively increasing rate up to 0.16 μg/kg/min to suppress endogenous pancreatic insulin and glucagon secretion (Seaquist et al., 1994). Dextrose (50% w/vol) was infused into the other arm vein at a variable rate adjusted to maintain target glycemia. Alterations in the glucose infusion rate were made based on the plasma glucose concentration measured by a nearby glucose analyzer (Beckman, Fullerton, CA, U.S.A.) in blood samples taken from the foot vein every 3–5 min. Additional blood samples were obtained every 10 min for the later determination of plasma insulin concentration and both before and after the study for assessment of plasma ketone concentrations.

Chemical assays

Insulin was quantified in serum that had been frozen within 30 min of acquisition using the double antibody method of Morgan and Lazarow (1963). Serum ketones were assessed in the clinical laboratory by a qualitative test based on the nitroferrocyanide reaction.

Magnetic resonance (MR) imaging (MRI)

All experiments were performed in a 4-T 125-cm bore magnet (Siemens/Varian). Subjects were positioned supine on the patient bed above the surface coil. After coil tuning, MRI was acquired using either FLASH (Haase et al., 1986) or MDEFT (Lee et al., 1995) to determine localization for spectroscopy according to anatomical landmarks. Subjects wore earplugs to minimize gradient noise and were placed into the coil holder using cushions to minimize head movement. Shimming of the identified region of interest was performed using FASTMAP (Gruetter, 1993), as described previously (Gruetter and Ugurbil, 1995), which resulted in water linewidths of 7–9 Hz and metabolite linewidths of 5–8 Hz.

^{1}H MR spectroscopy (MRS)

^{1}H MRS was performed inside a 33-cm head gradient providing 30 mT/m gradient strengths. The rise time was controlled by software and set to 250 μs. A 18-cm triple surface coil arrangement producing quadrature polarization (Merkle et al., 1993) was used for excitation and reception. The 3,1-DRY-STEAM modification of stimulated echo spectroscopy was used with an echo time TE of 20 ms, TM = 33 ms, and TR = 3 s as described previously (see Gruetter et al., 1996*b*, and references therein). Water suppression was achieved by using 25-ms-long Gaussian pulses at the water frequency, one of which was applied during the 33-ms-long TM period between the second and third slice selective pulses. Outer volume suppression in a plane adjacent to the volume at the coil surface was performed using BISTRO (deGraaf et al., 1995). The selected volume size was 27 ml ($3 \times 3 \times 3$ cm^3), which was confined to encompass the visual cortex, an area of consistently high metabolic activity and blood flow. The volume was placed symmetrically with respect to the brain midline, and the large veins were excluded by the position. Unwanted coherences were eliminated by placing two 5-ms-long crusher gradients (28.8 mT/m, 40 ms apart) in each TE period, which amounts to a

diffusion weighting factor b = 54 s/mm^2, thereby reducing the vascular signal by ~40% (Neil et al., 1994).

Spectra were obtained with a 1.5-min time resolution, which permitted retrospective summation of those intervals that followed a 20-min stabilization in plasma glucose level. Processing included extensive zero-filling, exponential multiplication corresponding to 2 Hz line broadening. Quantification of the glucose peak at 5.23 parts per million (ppm) was performed relative to the creatine (Cr) methyl resonance at 3.04 ppm as follows: To account for contributions of macromolecule resonances at 2.98 ppm, which are manifest in the 4-T spectra as an upfield shoulder of the Cr peak, two Lorentzian peaks were fitted simultaneously at 3.04 ppm and at 2.98 ppm. The linewidth of the latter peak was set to the sum of 11 Hz plus the linewidth of Cr. The glucose resonance was fitted to a Lorentzian curve whose linewidth was set to the Cr linewidth plus 2 Hz. Glucose concentration was calculated from the area of the glucose peak, I_{Glc}, and the area of the Cr peak, I_{Cr}, according to

$$[\mathrm{Glc}] = I_{Glc} * \frac{3[\mathrm{Cr}]_{tot}}{0.4 * I_{Cr}} \quad (1)$$

where the concentration of the total Cr intensity, $[\mathrm{Cr}]_{tot}$, was set to 10 mM, based on its cortical concentration of 9.6 mM (Petroff et al., 1989) and on contributions of 1 mM GABA in this region of the brain (Rothman et al., 1993). The residual was visually inspected to verify proper convergence of the peak fitting routine, which is a standard part of the spectrometer software. The transverse relaxation times of glucose and Cr were assumed to be identical, based on our previously reported T_2 of at least 90 ms (Gruetter et al., 1996*b*) and the similarity of the linewidth, when taking into account the contributions from J coupling. The saturation factors (due to the longitudinal relaxation times) were also assumed to be identical for both resonances, based on the observation that an inversion pulse applied before the beginning of the pulse sequence eliminates the glucose and the Cr resonance at the same inversion delay (data not shown) and that the TR of 3 s is ~2.5 times the T_1 of Cr at 4 T (Mason et al., 1994; Posse et al., 1995).

^{13}C MRS

^{13}C MRS was performed on a 4-T magnet using standard Siemens VISION body gradients, capable of providing 24 mT/m in 1.2 ms using a quadrature ^{1}H coil (12 cm in diameter) with a 7-cm diameter ^{13}C coil (Adriany and Gruetter, 1997). Localization was achieved with PRECISELY, which is a combination of ISIS localization (Ordidge et al., 1986) and DEPT polarization transfer methods (Doddrell et al., 1982), as described previously (Gruetter et al., 1996*a*). A 72-ml volume was selected to cover the occipital lobe based on FLASH imaging (TR = 60 ms, TE = 7 ms, 30° flip angle).

Data acquisition used a nominal DEPT editing pulse width, θ, of 90° for maximal sensitivity of the glucose C-1 through C-5 resonances. Editing delays were set for a heteronuclear J_{CH} coupling constant of 150 Hz. Pulse widths and power were calibrated on an external small sphere placed at the ^{13}C coil center containing [^{13}C] formic acid. ^{13}C pulse widths for a 180° pulse were determined by nulling the formate signal at resonance, and the ^{1}H pulse power for a 500-μs 90° pulse was determined using the method of Bax (1983). Pulse widths and power for the PRECISELY sequence were set according to the position relative to the coil based on previous calibrations. During acquisition (171 ms) WALTZ-16 decoupling was applied, which resulted in a 5.6% duty cycle (TR = 3 s) and an average power of <3 W, which is well within Food and Drug Administration guidelines for specific absorption rates.

Quantification of ^{13}C signals was performed using the external reference method as used in previous ^{13}C MRS studies of the human head (Gruetter et al., 1992*a*,*b*, 1994*b*) and verified by comparison with chemical extraction (Gruetter et al., 1991, 1994*a*; Taylor et al., 1992). In brief, the effect of variable coil loading on sensitivity was assessed by measuring the fully relaxed signal of the formic acid sphere. The glucose signal was quantified by performing the identical experiment on a 4-L phantom containing ~240 mM natural abundance glucose:

$$[\mathrm{Glc}] = \frac{I_{Glc}^{\text{in vivo}} * I_{FA}^{\text{ref}} * 240}{I_{Glc}^{\text{ref}} * I_{FA}^{\text{in vivo}}} \quad (2)$$

where I_{Glc} and I_{FA} represent glucose and formic acid signals, respectively. This calculation assumes that the saturation factors of glucose are identical in vivo and in solution, both of which were assessed to be within 10% of each other based on the similarity of T_1 of Cr and glucose in vivo and on the similar T_1 of glucose and Cr in solution. Signal differences due to differential T_2 were also neglected because the measured linewidth of 2–3 Hz suggests T_2 is >100 ms, which is much longer than the T_2 evolution time of the sequence (9 ms).

Kinetic modeling

It has become widely accepted that the physical distribution space of glucose at steady-state equals the brain water phase, which implies that intra- and extracellular glucose levels are similar, i.e., in the steady state, glucose is evenly distributed in the brain's aqueous phase based on animal (Pappenheimer and Setchell, 1973; Lund-Andersen, 1979; Gjedde and Diemer, 1983) and human (Gruetter et al., 1996*c*) studies. It has therefore become customary to assume a uniform brain glucose concentration past the blood–brain barrier, which is a foundation of the standard symmetric Michaelis–Menten model of brain glucose transport (Lund-Andersen, 1979). The model further assumes that *classic* Michaelis–Menten kinetics are valid to describe the unidirectional fluxes across the lumenal and ablumenal membrane. It has also become customary to assume symmetric kinetic constants for influx and efflux across the blood–brain barrier. Furthermore, it has been assumed that cerebral glucose consumption is constant at euglycemia and above, which is consistent with arteriovenous difference measurements and blood flow measurements in animals and humans (Pappenheimer and Setchell, 1973; Boyle et al., 1994). We have shown that cerebral glucose content at euglycemia is ~1 μmol/g wet weight in the human brain (Gruetter et al., 1992*a*), which is well above the K_m of brain hexokinase (50 μM), which further corroborated this assumption.

The standard Michaelis–Menten model was fitted to the measured steady-state brain glucose concentrations using the expression

$$G_{Brain} = V_d K_t \frac{\left(\frac{T_{max}}{CMR_{glc}} - 1\right) G_{plasma} - K_t}{\left(\frac{T_{max}}{CMR_{glc}} + 1\right) K_t + G_{plasma}} \quad (3)$$

The derivation of equations equivalent to Eq. 3 has been subject of several articles and many previous studies (Pappenheimer and Setchell, 1973; Gjedde and Diemer, 1983; Gjedde and Christensen, 1984; Gruetter et al., 1992*a*, 1993, 1996*c*; Mason et al., 1992). Brain glucose G_{brain} is given in μmol/g, the metabolic rates T_{max} and cerebral metabolic rate CMR_{glc} are given in μmol/g/min, and plasma glucose G_{plasma} and the Michaelis–Menten constant K_t are given in mM. The physical distribution space of glucose was assumed at V_d = 0.77 ml/g (Gjedde and Diemer, 1983; Holden et al., 1991; Gruetter et al., 1996*c*). It has been noted that including the endothelial compartment results in T_{max} being replaced by T_{max} * 0.5 without changing the algebraic form of Eq. 3, which may change the interpretation of T_{max} to being the maximal transport rate across the endothelial cell membranes (Pappenheimer and Setchell, 1973; Gjedde and Christensen, 1984; Mason et al., 1992). It is obvious from Eq. 3 that at saturating plasma glucose concentrations G_{brain} approaches the upper limit of $V_d K_t (T_{max}/CMR_{glc} - 1)$.

Reversible Michaelis–Menten kinetics are applicable when the product formation is not unidirectional (Mahler and Cordes, 1971; Cunningham et al., 1986). Such a situation is likely in vivo at metabolic steady state and amounts to replacing the Michaelis–Menten constant K_m by the term $K_m + P$ for product formation and, conversely, $K_m + S$ for the reverse reaction (Mahler and Cordes, 1971; Cunningham et al., 1986). This can be interpreted as reduced affinity for the forward reaction (influx) when substantial substrate (brain glucose) is present, a situation that would result in asymmetric kinetic properties.

As shown in Appendix, at steady state the reversible Michaelis–Menten model results in the expression

$$G_{brain} = V_d \frac{\left(\frac{T_{max}}{CMR_{glc}} - 1\right) G_{plasma} - K_t}{\frac{T_{max}}{CMR_{glc}} + 1} \quad (4)$$

which predicts that brain glucose content is a linear function of plasma glucose content when assuming a single membrane step. As shown in Appendix, including the endothelial compartment results in an algebraically identical expression that alters the value and interpretation of T_{max} similar to the modification of the standard model. In addition, using asymmetric kinetic constants also preserves the linear relationship, and hence we conclude that a linear relationship between plasma and brain glucose content is a general consequence of using the reversible formulation of Michaelis–Menten kinetics for the unidirectional transport rates.

Fitting of Eqs. 3 and 4 was performed using the Levenberg–Marquardt algorithm, and the error analysis was performed by a Monte–Carlo simulation of noise using Gaussian deviates whose root-mean-square amplitude was set such that the average deviation was equal to that of the actual fit to the in vivo data (Press et al., 1989). Statistical analysis was based on the covariance matrix provided by the fitting algorithm and the two-dimensional scatter plot of simulated parameter pairs in parameter space, which was analyzed for covariance among the values for K_t and T_{max}/CMR_{glc} and which was used to establish the statistically significant difference based on simulations using at least 2,000 trial data sets. To account for a potential contribution of blood glucose present in the cerebral blood volume (CBV) to the overall glucose signal, the data were also fitted to Eqs. 3 and 4 plus the term CBV * G_{plasma}. The effect of variable CBV was estimated by fitting G_{brain} − CBV * G_{plasma} to Eqs. 3 and 4 by systematically varying CBV between 0 and 0.075 ml/g.

RESULTS

All subjects were clamped at target glycemia for ≥20 min before spectroscopy was begun. Somatostatin infusion was tolerated well and suppressed endogenous insulin concentrations to <5 μU/ml (30 pM). Qualitative ketone level measurements were negative in all subjects. Proton MR spectra obtained from the occipital lobe at euglycemia and during a two-step hyperglycemic clamp are shown in Fig. 1A. The peak from the αH1 is clearly discernible at 5.23 ppm with at most a quadratically varying baseline due to residual water wings. Quantification of this signal was performed relative to the intensity of the Cr peak at 3.04 ppm obtained by Lorentzian fitting. The strong correlation of brain glucose concentration with plasma glucose concentration is clearly evident by visual inspection of the data presented in Fig. 1A. ^{13}C MR spectra were obtained in three subjects during extended periods of hyperglycemia, and a representative ^{13}C NMR spectrum is shown in Fig. 1B. Quantification of the ^{13}C NMR spectra was based on the external reference method, which gave a glucose concentration of 5.6 μmol/ml of brain volume for this spectrum. It is interesting to compare the intensity of the 3β,5β peak at 76.6 ppm, which corresponds to 1.2 ^{13}C concentration units, with the peak of *myo*-inositol plus glucose at 72.0 ppm, which corresponds to two or more ^{13}C concentration units. The former is approximately half the intensity of the latter peak at 72.0 ppm, providing a qualitative confirmation that the glucose concentration was ~6 μmol/ml of brain volume, assuming identical relative sensitivity and a 7 μmol/ml of volume *myo*-inositol concentration (Gruetter et al., 1992*b*; Kreis et al., 1993).

The plot of the brain glucose concentrations measured as a function of plasma glucose is shown in Fig. 2. Figure 2A shows the concentrations derived by ^{1}H MRS. Brain glucose concentration is linearly correlated with plasma glucose concentration, as indicated by the high correlation coefficient of 0.90 (n = 27), which indicated an extremely high statistical significance for a linear relationship ($p < 0.001$). Fitting a quadratic polynomial of the form $a + bx + cx^2$ gave a small c = −0.00178 ± 0.0041, which is not different from 0 ($p > 0.05$). The plot of residuals of a linear regression is shown in Fig. 2C and confirms the impression that a line adequately describes brain glucose content. To validate the ^{1}H MRS quantification, we compared the cerebral glucose concentration measured by ^{1}H MRS with that determined by ^{13}C MRS. The concentrations derived by ^{1}H MRS gave a brain glucose concentration of 6.8 ± 1.1 mM (mean ± SD) at 21.7 ± 1.9 mM in plasma (n = 3), whereas the brain

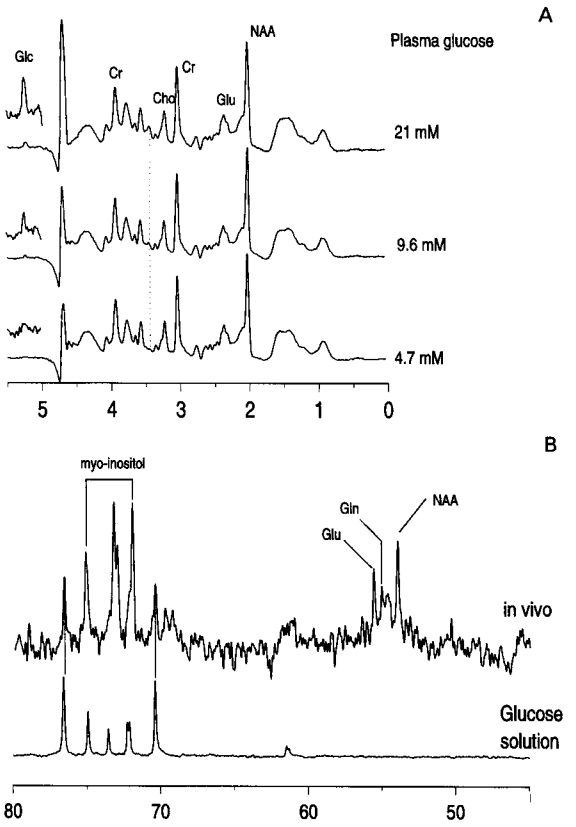

FIG. 1. ^{1}H and ^{13}C MRS of the human occipital lobe at 4 T. Shown are representative spectra obtained from the human visual cortex. **A:** Range of protons bound to aliphatic carbons. The **inset** at 5.1–5.5 ppm shows the vertically enlarged glucose peak at 5.23 ppm. The dotted line indicates the position of the resonances at 3.44 ppm that rise concomitantly. The spectra were acquired at plasma glucose concentrations of 4.7 (bottom), 9.6 (middle), and 21 m*M* (top) indicated to the right of the respective spectrum, and the corresponding quantification of the 5.23 ppm peak shown in the inset gave a brain glucose concentration of 1.2 (bottom), 2.4 (middle), and 5.5 μmol/g (top). **B:** The top spectrum shows a natural abundance spectrum acquired for 60 min from a 72-ml volume. The glucose resonances at 76.6 and 70.5 ppm were quantified by comparison with a phantom spectrum acquired at the same location under identical experimental parameters (bottom spectrum). Resonance assignments are based on estimated concentration and chemical shift (Willker et al., 1996). Glc, glucose; Glu, glutamate; Gln, glutamine; Cho, choline groups; NAA, *N*-acetylaspartate. Spectra were processed with a mild Lorentz to Gauss apodization (3 Hz) and are shown without baseline correction.

glucose concentration by natural abundance ^{13}C MRS was 6.9 ± 0.9 m*M* at 21.9 ± 1.8 m*M* in plasma (n = 3).

The fit of the present data to the standard symmetric Michaelis–Menten model of blood–brain glucose transport (Lund-Andersen, 1979; Gjedde and Christensen, 1984; Holden et al., 1991; Gruetter et al., 1992*a*; Mason et al., 1992) results in the solid line in Fig. 2A and in K_t = 9.0 ± 2.4 m*M* and T_{max}/CMR_{glc} = 4.5 ± 0.3 with a χ^2 = 38. The errors were determined using a Monte–Carlo simulation with a 1.15

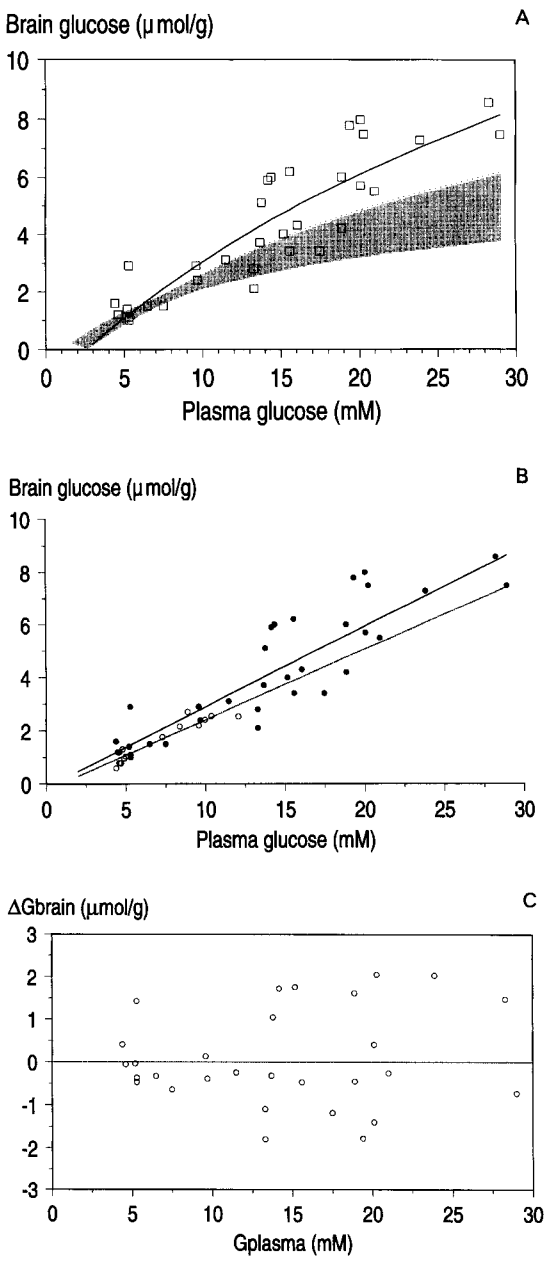

FIG. 2. Relationship between plasma and brain glucose concentration. **A:** Brain glucose concentrations measured by ^{1}H MRS (open squares). The solid line is the best fit of the standard Michaelis–Menten model (Eq. 3) to the brain glucose concentrations determined by ^{1}H MRS. The shaded area represents the 95% confidence interval of extrapolated steady-state cerebral glucose concentrations calculated from previously published data using Eq. 3 and the kinetic parameters K_t = 4.9 ± 0.8 m*M* and T_{max}/CMR_{glc} = 3.56 ± 0.2 (Gruetter et al., 1992*a*, 1993). **B:** Data from this study (●) and from the previous ^{13}C MRS study (○). The corresponding best fit of the reversible Michaelis–Menten model using Eq. 4 to the data from this study is the solid (upper) line, whereas the dotted (lower) line is the best fit of Eq. 4 to the data from the previous ^{13}C MRS study. The resulting fit parameters are given in Table 2. **C:** Residuals of fitting a line to the brain glucose level measurements of this study, $\Delta G_{brain} = G_{brain}^{measured} - G_{brain}^{fitted}$, which is equivalent to using Eq. 4. Note the absence of any significant trend of the residuals with plasma glucose concentration.

TABLE 1. *Michaelis–Menten constants for glucose transport in the human brain derived with the symmetric model*

	Method	No. of subjects	Plasma glucose range studied (mM)	K_t (mM)	T_{max} (μmol/g/min)	$\frac{T_{in} - \text{maximum CMR}_{glc}}{\text{CMR}_{glc}}$ (%)
Brooks et al. (1986)	PET	4	3.9–5.7	4.2	0.4	−28
Feinendegen et al. (1986)	PET	6	2.7–7.7	3.8	2.0	272
Gutniak et al. (1990)	PET	8	2.7–6.0	4.1[a]	0.5[a]	−23
Blomqvist et al. (1991)	PET	8	2.7–6.0	4.1	0.6	8
Gruetter et al. (1992*a*)	NMR	7	4.8–13	4.8	1.1	83
Gruetter et al. (1996*c*)	NMR	5	4.8–19	4.9	1.0	65
Present study	NMR	23	4.6–30	9.0	1.3	48

[a] Derived by fitting $k_1 = T_{max}/(K_t + G_{plasma})$ to k_1 measured at two different G_{plasma} values.

mM root-mean-square noise level. Assuming the accepted standard for gray matter glucose consumption CMR_{glc} of 0.3 μmol/g/min (Heiss et al., 1984), these kinetic constants yield a maximal transport rate T_{max} of 1.3 ± 0.1 μmol/g/min, which is 25% above the previously reported values (Gjedde, 1992; Gruetter et al., 1996*c*) (Table 1). Inspection of the generated two-dimensional Monte–Carlo scatter plots spanning the parameter space showed that this set of kinetic constants is significantly ($p < 0.01$) different from that previously published (Gruetter et al., 1992*a*). Furthermore, the covariance of the two parameters was 0.28 for the previous study and −0.42 for the present study ($p > 0.05$). Visual inspection of the parameter space confirmed the absence of any strong covariance. Moreover, all the glucose concentrations measured at plasma glucose concentrations >20 mM were significantly >5 μmol/g. Brain glucose concentration was 8.6 μmol/g at 28.3 mM plasma glucose concentration, which implies that at 30 mM, the brain glucose concentration approaches 9 μmol/g (Fig. 2). The shaded area in Fig. 2A shows the 95% confidence area of the predicted relationship between plasma and brain glucose concentrations based on the kinetic constants calculated in previous ^{13}C MRS studies of glucose transport in the human brain (Gruetter et al., 1992*a*, 1993; see also row 6 in Table 1). The 95% confidence area was determined from the extreme brain glucose concentrations calculated over the previously reported 95% confidence intervals of K_t and T_{max}/CMR_{glc}. These previously reported constants were consistent with the average constants derived in PET studies (Gjedde, 1992) in which the standard symmetric Michaelis–Menten model of brain glucose transport was also used (Table 1). Despite the observed differences between the current and the extrapolated curve based on previously published kinetic constants, the experimental data presented in this study are in excellent agreement with these previous studies, all of which were measured at plasma glucose concentrations between 5 and 15 mM. The agreement is further illustrated by the overlap between the shaded area and the present measurements (Fig. 2A, open squares).

The measurement of brain glucose concentrations substantially above the K_m of GLUT-1 in the human brain indicates that the E + P → EP reaction may proceed at significant rates and that glucose binding at the ablumenal side may partially inhibit the unidirectional influx. To evaluate whether incorporating such a mechanism can accommodate these measurements more consistently, we fitted the reversible Michaelis–Menten model using Eq. 4, which resulted in $K_t = 0.6 \pm 2.0$ mM and $T_{max}/\text{CMR}_{glc} = 2.3 \pm 0.2$. The resulting parameters are shown in Table 2, and the corresponding best fit (solid line) is shown in Fig. 2B. The residuals of this best fit (a line by definition) are shown in Fig. 2C, and they indicate the absence of any trend in the residuals. To determine whether the previous ^{13}C MRS quantification can predict the high brain glucose values observed when using the reversible model, we fitted Eq. 4 also to the data reported by Gruetter et al. (1993), which are replotted in Fig. 2B (open circles). Unlike the case with the symmetric (irreversible) Michaelis–Menten kinetic model, however, when Eq. 4 was fitted to the previously reported ^{13}C MRS quantification, the dashed line in Fig. 2B was obtained, which is a much better extrapolation of brain glucose values to the present study than that achieved from the standard model (dashed curve in Fig. 2A). The parameters of this fit are given in Table 2.

To assess the influence of neglecting a vascular signal component to the MR signal of brain glucose, we varied the CBV in the fit of Eqs. 3 and 4. The resulting parameters are shown in Table 3. The effect of progressively increasing the contribution of vascular signal to the MR signal was to produce a modest decrease in K_t and T_{max} in the fit of either model of blood–brain barrier transport. Linear regression analysis (bottom row) revealed that either parameter increased by 2% per 0.01 ml of underestimated blood volume/g.

DISCUSSION

In this investigation, we have measured cerebral glucose concentrations under controlled conditions at levels of glycemia never before studied in healthy human subjects. The present measurements of cerebral glucose content were found to be in excellent agreement

TABLE 2. *Michaelis–Menten constants derived using the reversible model*

	Method	No. of studies	Plasma glucose range studied (m*M*)	K_t (m*M*)	T_{max} (μmol/g/min)
^{13}C MRS[a]	^{13}C NMR	7	4.8–13	0.96	0.62
Present study	^{1}H NMR	23	4.6–29	0.6 ± 2.0	0.69 ± 0.09

[a] Calculated by fitting Eq. 4 to the data reported by Gruetter et al. (1992*a*, 1993).

over the same ranges of moderate hyperglycemia used in previous studies. Our data were obtained by proton spectroscopy and confirmed by ^{13}C MRS.

We found that a linear relationship exists between plasma and brain glucose concentrations over the range of plasma glucose concentration used in this study, i.e., 4–30 m*M*. This linearity is directly illustrated in Fig. 1A, where the brain glucose signal increases in parallel with plasma glucose level. Certainly those data, as well as the plots in Fig. 2, do not provide any evidence for an asymptotic upper limit of brain glucose level between 4 and 30 m*M* plasma glucose, as required by the standard model. Further insight that a linear relationship describes brain glucose content is provided by fitting the standard model to the data points projected onto the linear regression curve, which assumes zero noise. The fit provided $K_t = 4.8$ and $T_{max}/CMR_{glc} = 3.63$ for the previous ^{13}C data and $K_t = 8.9$ and $T_{max}/CMR_{glc} = 4.5$ for the present study. These parameters are almost identical to those reported from the fit to the actual data reported above and mathematically reflect that the standard model attempts to mimic linear data acquired over a finite range of glycemia. Therefore, if a plateau exists as the standard model would predict, it is at a plasma glucose level well above 30 m*M*, which is at least an order of magnitude above the apparent K_m reported for the erythrocyte carrier protein GLUT-1. We therefore conclude that the failure to extrapolate from a lower range of plasma glucose content measured does not stem from the underestimation of a very high K_m of glucose transport. Therefore, the only instance where the standard model is compatible with a linear relationship is when metabolism, CMR_{glc}, is negligible compared with transport, T_{max}. In such a situation brain glucose concentration would equal plasma glucose concentration, a condition that is clearly not present in normal brain. The observation of a linear relationship implies that many models previously used to describe the kinetics of cerebral glucose transport may not be adequate. Our data were best fit by a reversible Michaelis–Menten model where product formation is not a unidirectional process. Therefore, we conclude that cerebral glucose concentration may have a direct effect on the rate of unidirectional glucose uptake into the human brain.

The measurement of cerebral glucose content by MRS is a direct, noninvasive approach that measures average tissue content of the metabolite. Even though we have taken great care that the signal was selected from a volume element that did not include any major veins, some contribution of the signal in smaller microscopic vessels cannot be ruled out. However, based on the simulations presented in Table 3, the assumption that 5% of cerebral volume is occupied by blood decreases the derived kinetic parameters by at most 10% and does not change the observed linearity of the blood–brain glucose relationship. It should also be noted that the present pulse sequence uses strong crusher gradients and induces some diffusion and perfusion weighting. Based on published measurements of attenuation of blood signal using ^{19}F MRS of fluorinated compounds in blood, the present b value of 54 s/mm^2 is expected to attenuate the blood signal by ~40% (Neil et al., 1994). Assuming that glucose in blood has a similar sensitivity to gradient dephasing as that in water, including the vascular signal decreases the kinetic constants by at most 6%, which is well within the experimental uncertainty of the present study.

TABLE 3. *Effect of vascular glucose signal on kinetic parameter estimation*

	Reversible model		Standard model	
CBV (% volume)	K_t (m*M*)	$\frac{T_{max}}{CMR_{glc}}$	K_t (m*M*)	$\frac{T_{max}}{CMR_{glc}}$
0	0.00	0.00	0.00	0.00
2.5	−0.15	−0.09	−0.06	−0.07
5	0.06	−0.13	−0.09	−0.16
7.5	−0.15	−0.17	−0.16	−0.23
Relative slope (% change per 0.01 ml/g CBV)	2.0	2.4	2.1	3.0

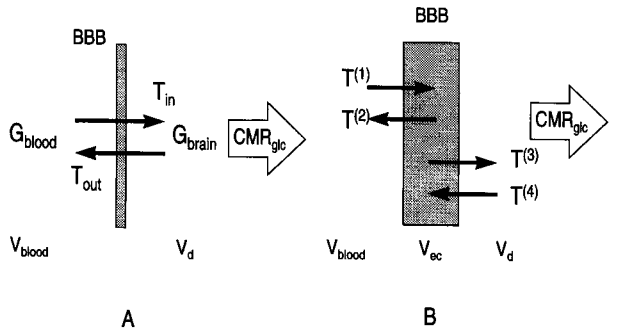

FIG. 3. Model of reversible Michaelis–Menten kinetics. The steady-state model assumes that past the blood–brain barrier (BBB), glucose is evenly distributed in the brain's aqueous phase (Lund-Andersen, 1979; Gjedde and Diemer, 1983; Holden et al., 1991; Mason et al., 1992) and that glucose consumption CMR_{glc} is unaffected by changes in plasma glucose concentration over the range of glycemia studied. The model in **A** neglects the effect of the endothelial cell compartment, which is accounted for in model **B**. The unidirectional transport rates T are modeled assuming reversible Michaelis–Menten kinetics, given by expressions analogous to Eq. 4.

Kinetic models of steady-state blood–brain barrier glucose transport have been based on two models (Fig. 3). The simpler model neglects the endothelial cell compartment (Fig. 3A) and requires two unidirectional fluxes, T_{in} and T_{out}, which are traditionally modeled using *standard* Michaelis–Menten kinetics. The more general model (Fig. 3B) includes the effect of a very small but finite endothelial cell compartment with negligible metabolism and with four concomitant unidirectional fluxes $T^{(i)}$. Traditionally symmetric kinetic constants on both sides of the membrane are assumed. We show in Appendix that inclusion of the endothelial compartment yields also expressions algebraically equivalent to Eq. 4 (see Appendix for the derivation of reversible kinetics). However, a difference exists relative to the analogous expressions for the standard model (Pappenheimer and Setchell, 1973; Gjedde and Christensen, 1984; Mason et al., 1992), because the intercept and the slope are affected whether the endothelial cells are explicitly modeled, as can be seen by comparing Eq. A10 with Eq. A5. Recalculating the kinetic parameters using Eq. A10 gave $T_{max}/CMR_{glc} = 4.4$ and $K_t = 0.5$ mM. The relative transport rate thus is doubled, which can be interpreted as representing the transport capacity across one endothelial membrane as in the case for the standard model. Note that K_t is only minimally affected.

The linear relationship between plasma glucose and brain glucose concentrations is a robust feature of our brain glucose level quantification because neither potential quantification errors nor a vascular contribution to the signal alters the linearity of the curve (Fig. 2) or any of the model assumptions.

The present observation of a linear brain glucose concentration curve is consistent with earlier reports suggesting the presence of a high-affinity low-capacity transport system (Gjedde, 1981) or a nonsaturable transport mechanism (Pardridge, 1983), as both mechanisms give rise to a linear relationship as well. Therefore, we cannot, based on our measurements, exclude the presence of such a mechanism, although it remains to be determined how using the reversible Michaelis–Menten kinetic formulation may affect interpretation of tracer passage and extraction measurements, and whether the increase with plasma glucose concentration of the apparent K_t in the reversible model would be sufficient to explain these previous observations, because the apparent K_m for unidirectional influx is equal to the sum of K_t and G_{brain}. It is interesting to note that a similar analysis of kinetic tracer experiments in rat brain suggested that the difference of the two models may manifest itself as such a nonsaturable component (Cunningham, 1986).

The present study is in agreement with previous measurements of brain glucose levels in animal brain using standard kinetics, as can be seen by visual inspection of graphs provided by Gjedde and Christensen (1984) and by Mason et al. (1992), as well as by Holden et al. (1991), who reported a K_t of 9–14 mM using the standard model, a value that is in excellent agreement with the present fit using the standard model (Table 2). It is interesting to note that these studies measured a K_t that is markedly higher than the K_m measured in erythrocyte model systems against a zero intracellular glucose concentration (Carruthers, 1990). A similar analysis of tracer kinetic data reported also a millimolar K_t in rat brain (Cunningham et al., 1986), but a different study suggested that analyzing brain glucose content as a function of plasma glucose content using the standard model gave a K_t of 14 mM in *rat* brain (Mason et al., 1992). Such a high K_t can be taken as an indication of an almost linear brain–blood glucose relationship.

Some studies have suggested that although the human GLUT-1 has anomalous asymmetric kinetic properties, most mammalian erythrocyte kinetics are symmetric (Cloherty et al., 1996). Nevertheless, we show in Appendix that the linear relationship between brain and plasma glucose levels using reversible Michaelis–Menten kinetics is preserved even when assuming asymmetric kinetic properties. Because the model is thus underdetermined and most evidence suggests transport symmetry (see, e.g., Gjedde and Diemer, 1983), we assumed the transporter to be symmetric and refer to the derived kinetic constants as apparent constants of transport, K_t and T_{max}.

The present modeling of glucose transport includes reversible kinetics, i.e., adds the reverse reaction E + P $\rightarrow$ EP, which substantially reduces the intrinsic K_t of glucose transport because increased product concentration decreases the apparent affinity for substrate binding. Such a behavior is expected for the glucose transporter GLUT-1, as it has been shown that cytochalasin B, which binds to the efflux binding site, increases the K_i for maltose binding at the sugar influx site of the

carrier (Carruthers and Helgerson, 1991). Furthermore, by comparing our measurements of brain glucose levels over an extended range of plasma glucose levels with those previously reported over a much narrower plasma glucose level range (Gruetter et al., 1992*a*), we obtained apparent Michaelis–Menten constants T_{max} and K_t that are in excellent agreement and thus appear to be independent of the range of glucose levels studied.

We finally note that the glucose transporter abundant at the blood–brain barrier and that in the human erythrocyte have been ascribed to the same transporter, i.e., the ubiquitous GLUT-1. In studies of erythrocyte model systems the Michaelis–Menten constant has been measured to be 0.5–2.0 m*M* against a zero glucose concentration inside (Carruthers, 1990), which is in excellent agreement with the present study.

The maximal net glucose transport capacity across the blood–brain barrier at euglyemia can be estimated from the measured kinetic constants. Net glucose transport into the brain is maximal when brain glucose G_{brain} falls into the range of the K_m of hexokinase, which is ~50 μM. The *sustainable* maximal glucose metabolic rate, CMR_{glc}, is in this case determined by the unidirectional influx, and the relative increase that is possible in the presence of an excess of basal CMR_{glc} is given in the last column of Table 1. The maximal sustainable rate of glucose uptake was calculated from

$$\text{maximum } T_{in} = T_{max} \frac{G_{plasma}}{K_t + G_{plasma}} \qquad (5)$$

which is valid for both types of Michaelis–Menten kinetics discussed in this article, as can be seen from Eq. A3 in Appendix and the well-known formulations for the standard model (Lund-Andersen, 1979; Pardridge, 1983; Gjedde, 1992; Gruetter et al., 1996*c*). It is interesting to note that the high K_t of 9 m*M* implies that the maximal net glucose transport capacity at the blood–brain barrier is 48% above the resting glucose consumption, which is similar to the glucose consumption rate measured during photic stimulation (Fox et al., 1988). The low K_t of ~1 m*M* derived by fitting the reversible Michaelis–Menten kinetic model implies that the maximal glucose uptake capacity is close to T_{max} for most physiological plasma glucose concentrations in humans. At euglycemia the maximal sustainable metabolic rate of glucose is 71 or 94% in excess of the basal rate of glucose combustion, as can be calculated from Table 2 using Eq. 5. These values easily accommodate most measured increases of CMR_{glc} under physiological stimulation in the human occipital lobe, where the present study has been performed.

We conclude that the similarity of in vivo kinetic parameters with in vitro kinetic constants of GLUT-1 supports the observation that the abundant cerebral glucose transporter at the blood–brain barrier is GLUT-1. Based on the quantification provided by ^1H and ^{13}C spectroscopy in this study and their excellent agreement with an independent study previously reported (Gruetter et al., 1992*a*), the reversible Michaelis–Menten model describes steady-state brain glucose concentrations in the human brain consistently and allows for a transport capacity that is well in excess of observed physiological increases in cerebral metabolism.

Acknowledgment: This work was supported by U.S. Public Health Service Grants RR08079 and RR00400 from the National Center for Regional Resources of the National Institutes of Health and by the Juvenile Diabetes Foundation. We thank Drs. Douglas Rothman and Robert Shulman for pointing out the article by Mahler and Cordes (1971).

APPENDIX

Calculation of asymmetric kinetic constants and of endothelial compartment

This section demonstrates that the linear relationship between glucose inside and glucose outside is a general consequence of reversible Michaelis–Menten kinetics. First, we derive the expression analogous to Eq. 4 but assume a more general case that allows asymmetric transport kinetics for the individual unidirectional fluxes. Consequently, inclusion of the endothelial double membrane compartment does not change the linearity of the relationship between steady-state brain and plasma glucose.

The model of glucose transport is shown in Fig. 3A. At steady state, mass conservation requires that the unidirectional influx T_{in} equals the sum of efflux T_{out} and consumption CMR_{glc}, all of which are given in μmol/g/min, i.e.,

$$T_{in} = T_{out} + CMR_{glc} \qquad (A1)$$

Glucose transport at *steady state* described by *reversible* Michaelis–Menten kinetics is given in Eq. A2, where E denotes the transporter, P the *trans*-membrane glucose, and S the *cis*-membrane glucose

$$E + S \leftrightarrow ES \leftrightarrow EP \leftrightarrow E + P \qquad (A2)$$

Standard Michaelis–Menten kinetics assume the last step to proceed unidirectionally toward product (P) formation. The expressions for the reaction proceeding in either direction, i.e., influx or efflux, are given by expressions according to that given for T_{in} (Mahler and Cordes, 1971; Cunningham et al., 1986) in Eq. A3:

$$T_{in} = T_{max} \frac{G_{plasma}}{K_t + G_{plasma} + G_{brain}/V_d} \qquad (A3)$$

and, conversely,

$$T_{out} = T_{max} \frac{G_{brain}}{V_d K_t + G_{brain} + V_d G_{plasma}} \qquad (A4)$$

where K_t and G_{plasma} are given in m*M*, G_{brain} is in μmol/g, and V_d is the physical distribution space of glucose in the human brain. V_d was suggested in animal (Gjedde and

Diemer, 1983; Holden et al., 1991; Gjedde, 1992) and human (Gruetter et al., 1996*c*) brain to be close to the aqueous phase of the brain, i.e., 0.77 ml/g, which is supported by a comparable interstitial glucose concentration (Silver and Erecińska, 1994). By inserting the appropriate expressions into Eq. A1 we arrive at Eq. 4, which can be rewritten as

$$G_{brain} = V_d \frac{\left(\frac{T_{max}^2}{CMR^2_{glc}} - 1\right) G_{plasma} - K_t \left(\frac{T_{max}}{CMR_{glc}} + 1\right)}{\left(\frac{T_{max}}{CMR_{glc}} + 1\right)^2} \quad (A5)$$

which describes brain glucose content assuming reversible transport based on symmetric kinetic properties.

In the above analysis we have neglected the endothelial cell compartment, which shall now be evaluated together with the potential asymmetric kinetic constants to establish that a linear relationship between brain and plasma glucose concentrations is a general consequence of using reversible kinetics. Expressing influx into the endothelial cell as $T^{(1)}$, efflux into the blood as $T^{(2)}$, influx from the endothelial cell into the brain as $T^{(3)}$, and efflux from the brain into the endothelial cell as $T^{(4)}$, assuming that CMR_{glc} inside the brain is constant (Fig. 3B), the steady-state conditions require that

$$T^{(3)} = T^{(4)} + CMR_{glc} \quad (A6)$$

and

$$T^{(1)} + T^{(4)} = T^{(2)} + T^{(3)} \quad (A7)$$

This treatment is similar to that given by Cunningham et al. (1986) for tracer uptake experiments. Expressing $T^{(3)}$ and $T^{(4)}$ in terms of the steady-state endothelial glucose concentration, G_{ec}, and brain glucose concentration, G_{brain}, e.g.,

$$T^{(3)} = T^{(3)}_{max} \frac{G_{ec}}{K_t^{(3)} + G_{ec} + G_{brain}} \quad (A8)$$

and, conversely, for $T^{(4)}$. Solving Eq. A6 for G_{ec} yields

$$G_{ec} = \frac{(T^{(4)}_{max} K_t^{(3)} + CMR_{glc} K_t^{(4)})\, G_{brain} + CMR_{glc}\, K_t^{(3)} K_t^{(4)}}{T^{(3)}_{max} K_t^{(4)} - CMR_{glc} K_t^{(3)}} \quad (A9)$$

which is then substituted in the corresponding expressions in Eq. A7. It is interesting to note that because G_{ec} is a linear function of G_{brain} in Eq. A9, the same holds true for G_{brain} as a function of G_{ec} and thus also G_{brain} as a function of G_{plasma}. Hence, Eq. A9 shows that in the most general case of asymmetric transport constants, the relationship between inside and outside sugar is linear if reversible Michaelis–Menten kinetics are assumed. As a linear relationship can be completely described by its slope and y-intercept, the system is mathematically underdetermined. We have hence assumed glucose transport to be symmetric across the cell membranes, which is consistent with animal erythrocyte glucose transport kinetics and possibly kinetics of human erythrocytes (Cloherty et al., 1996).

Therefore, assuming symmetric transport properties for all membranes at the endothelial cell, the expression

$$G_{brain} = V_d \frac{\left(\frac{T_{max}}{CMR_{glc}} - 1\right)^2 G_{plasma} - K_t \left(\frac{2T_{max}}{CMR_{glc}}\right)}{\left(\frac{T_{max}}{CMR_{glc}} + 1\right)^2} \quad (A10)$$

is derived for brain glucose, which describes the kinetic effect of accounting for double-membrane transport kinetics across the endothelial compartment, as previously derived for the standard Michaelis–Menten model (Pappenheimer and Setchell, 1973).

REFERENCES

Adriany G. and Gruetter R. (1997) A half volume coil for efficient proton decoupling in humans at 4 Tesla. *J. Magn. Reson.* **125,** 178–184.

Bax A. (1983) A simple method for the calibration of the decoupler radiofrequency field strength. *J. Magn. Reson.* **52,** 76–80.

Blomqvist G., Gjedde A., Gutniak M., Grill V., Widén L., Stone-Elander S., and Hellstrand E. (1991) Facilitated transport of glucose from blood to brain in man and the effect of moderate hypoglycemia on cerebral glucose utilization. *Eur. J. Nucl. Med.* **18,** 834–837.

Boyle P., Nagy R., O'Connor A., Kempers S., Yeo R., and Qualls C. (1994) Adaptation in brain glucose uptake following recurrent hypoglycemia. *Proc. Natl. Acad. Sci. USA* **91,** 9352–9356.

Brooks D., Gibbs J., Sharp P., Herold S., Turton D., Lthra S., Kohner E., Bloom S., and Jones T. (1986) Regional cerebral glucose transport in insulin-dependent diabetic patients studied using [^{11}C]3-*O*-methyl-D-glucose and positron emission tomography. *J. Cereb. Blood Flow Metab.* **6,** 240–244.

Carruthers A. (1990) Facilitated diffusion of glucose. *Physiol. Rev.* **70,** 1135–1176.

Carruthers A. and Helgerson A. (1991) Inhibitions of sugar transport produced by ligands binding at opposite sides of the membrane. Evidence for simultaneous occupation of the carrier by maltose and cytochalasin B. *Biochemistry* **30,** 3907–3915.

Cloherty E., Heard K., and Carruthers A. (1996) Human erythrocyte sugar transport is incompatible with available carrier models. *Biochemistry* **35,** 10411–10421.

Crone C. (1965) Facilitated transfer of glucose from blood into brain tissue. *J. Physiol. (Lond.)* **181,** 103–113.

Cunningham V. (1986) The influence of transport and metabolism on brain glucose content. *Ann. NY Acad. Sci.* **481,** 161–173.

Cunningham V., Hargreaves R., Pelling D., and Moorhouse S. (1986) Regional blood–brain glucose transfer in the rat: a novel double-membrane kinetic analysis. *J. Cereb. Blood Flow Metab.* **6,** 305–314.

deGraaf R., Luo Y., Terpstra M., and Garwood M. (1995) Spectral editing with adiabatic pulses. *J. Magn. Reson. B* **109,** 184–193.

Doddrell D. M., Pegg D. T., and Bendall M. R. (1982) Distortionless enhancement of NMR signals by polarization transfer. *J. Magn. Reson.* **48,** 323–327.

Feinendegen L., Herzog H., Wieler H., Patton D., and Schmid A. (1986) Glucose transport and utilization in the human brain: model using carbon-11 methylglucose and positron emission tomography. *J. Nucl. Med.* **27,** 1867–1877.

Fox P., Raichle M., Mintun M., and Dence C. (1988) Nonoxidative glucose consumption during focal physiologic neural activity. *Science* **241,** 462–464.

Gerhart D., Broderius M., Borson N., and Drewes L. (1992) Neurons and microvessels express the brain glucose transporter protein GLUT3. *Proc. Natl. Acad. Sci. USA* **89,** 733–737.

Gjedde A. (1981) High- and low-affinity transport of D-glucose from blood to brain. *J. Neurochem.* **36,** 1463–1471.

Gjedde A. (1992) Blood–brain glucose transfer, in *Physiology and Pharmacology of the Blood–Brain Barrier* (Bradbury M., ed), pp. 65–117. Springer-Verlag, New York.

Gjedde A. and Christensen O. (1984) Estimates of Michaelis–Menten constants for the two membranes of the brain endothelium. *J. Cereb. Blood Flow Metab.* **4,** 241–249.

Gjedde A. and Diemer N. (1983) Autoradiographic determination of regional brain glucose content. *J. Cereb. Blood Flow Metab.* **3,** 303–310.

Gruetter R. (1993) Automatic, localized in vivo adjustment of all first- and second-order shim coils. *Magn. Reson. Med.* **29,** 804–811.

Gruetter R. and Ugurbil K. (1995) A fast, automatic shimming technique by mapping along projections (FASTMAP) at 4 Tesla, in *3rd Ann. Proc. Int. Soc. Magn. Reson. Med.,* Nice, France, p. 698.

Gruetter R., Prolla T., and Shulman R. (1991) ^{13}C-NMR visibility of rabbit muscle glycogen in vivo. *Magn. Reson. Med.* **20,** 327–332.

Gruetter R., Novotny E. J., Boulware S. D., Rothman D. L., Mason G. F., Shulman G. I., Shulman R. G., and Tamborlane W. V. (1992*a*) Direct measurement of brain glucose concentrations in humans by ^{13}C NMR spectroscopy. *Proc. Natl. Acad. Sci. USA* **89,** 1109–1112.

Gruetter R., Rothman D. L., Novotny E. J., and Shulman R. G. (1992*b*) Localized ^{13}C NMR spectroscopy of *myo*-inositol in the human brain in vivo. *Magn. Reson. Med.* **25,** 204–210.

Gruetter R., Novotny E., Boulware S., Rothman D., Mason G., Shulman G., Shulman R., and Tamborlane W. (1993) Non-invasive measurements of the cerebral steady-state glucose concentration and transport in humans by ^{13}C magnetic resonance, in *Frontiers in Cerebral Vascular Biology: Transport and Its Regulation* (Drewes L. and Betz A., eds), pp. 35–40. Plenum Press, New York.

Gruetter R., Magnusson I., Rothman D. L., Avison M. J., Shulman R. G., and Shulman G. I. (1994*a*) Validation of ^{13}C NMR determination of liver glycogen in vivo. *Magn. Reson. Med.* **31,** 583–588.

Gruetter R., Novotny E. J., Boulware S. D., Mason G. F., Rothman D. L., Shulman G. I., Prichard J. W., and Shulman R. G. (1994*b*) Localized ^{13}C NMR spectroscopy in the human brain of amino acid labeling from D-[1-^{13}C]glucose. *J. Neurochem.* **63,** 1377–1385.

Gruetter R., Adriany G., Merkle H., and Andersen P. M. (1996*a*) Broadband decoupled, ^{1}H localized ^{13}C MRS of the human brain at 4 Tesla. *Magn. Reson. Med.* **36,** 659–664.

Gruetter R., Garwood M., Ugurbil K., and Seaquist E. R. (1996*b*) Observation of resolved glucose signals in ^{1}H NMR spectra of the human brain at 4 Tesla. *Magn. Reson. Med.* **36,** 1–6.

Gruetter R., Novotny E. J., Boulware S. D., Rothman D. L., and Shulman R. G. (1996*c*) ^{1}H NMR studies of glucose transport in the human brain. *J. Cereb. Blood Flow Metab.* **16,** 427–438.

Gruetter R., Ugurbil K., and Seaquist E. R. (1996*d*) Steady-state cerebral glucose transport kinetics in humans by ^{1}H MRS. (Abstr.) *MAGMA* **4** (Suppl. 2), 138.

Gutniak M., Blomqvist G., Widen L., Stone-Elander S., Hamberger B., and Grill V. (1990) D-[U-^{11}C]Glucose uptake and metabolism in the brain of insulin-dependent diabetic subjects. *Am. J. Physiol.* **258,** E805–E812.

Haase A., Frahm J., Matthaei D., Hänicke W., and Merboldt K. D. (1986) FLASH imaging. Rapid NMR imaging using low flip-angle pulses. *J. Magn. Reson.* **67,** 258–266.

Heiss W., Pawlik G., Herholz K., Wagner R., Göldner H., and Wienhard K. (1984) Regional kinetic constants and cerebral metabolic rate for glucose in normal human volunteers determined by dynamic positron emission tomography of [^{18}F]-2-fluoro-deoxy-D-glucose. *J. Cereb. Blood Flow Metab.* **4,** 212–223.

Holden J., Mori K., Dienel G., Cruz N., Nelson T., and Sokoloff L. (1991) Modeling the dependence of hexose distribution volumes in brain on plasma glucose concentration: implications for estimation of the local 2-deoxyglucose lumped constant. *J. Cereb. Blood Flow Metab.* **11,** 171–182.

Kalaria R., Gravina S., Schmidley J., Perry G., and Harik S. (1988) The glucose transporter of the human brain and blood–brain barrier. *Ann. Neurol.* **24,** 757–764.

Knudsen G., Pettigrew K., Paulson O., Hertz M., and Patlak C. (1990) Kinetic analysis of blood–brain barrier transport of D-glucose in man: quantitative evaluation in the presence of tracer backflux and capillary heterogeneity. *Microvasc. Res.* **39,** 28–49.

Kreis R., Ernst T., and Ross B. (1993) Development of the human brain: in vivo quantification of metabolite and water content with proton magnetic resonance spectroscopy. *Magn. Reson. Med.* **30,** 424–437.

Le Fevre P. (1961) Sugar transport in the red blood cell: structure activity relationships in substrates and antagonists. *Pharmacol. Rev.* **16,** 39–70.

Lee J. H., Garwood M., Menon R., Adriany G., Andersen P., Truwit C. L., and Ugurbil K. (1995) High contrast and fast three-dimensional imaging at high fields. *Magn. Reson. Med.* **34,** 308–312.

Lund-Andersen H. (1979) Transport of glucose from blood to brain. *Physiol. Rev.* **59,** 305–352.

Maher F., Vannucci S., and Simpson I. (1993) Glucose transporter isoforms in brain: absence of GLUT3 from the blood–brain barrier. *J. Cereb. Blood Flow Metab.* **13,** 342–345.

Mahler H. and Cordes E. (1971) *Biological Chemistry.* Harper & Row, New York.

Mason G., Behar K., Rothman D., and Shulman R. (1992) NMR determination of intracerebral glucose concentration and transport kinetics in rat brain. *J. Cereb. Blood Flow Metab.* **12,** 448–455.

Mason G., Pan J., Ponder S., Twieg D., Pohost G., and Hetherington H. (1994) Detection of brain glutamate and glutamine in spectroscopic images at 4.1T. *Magn. Reson. Med.* **32,** 142–145.

Merkle H., Garwood M., and Ugurbil K. (1993) Dedicated circularly polarized surface coil assemblies for brain studies at 4 T, in *12th Annual Scientific Meeting of the Society for Magnetic Resonance in Medicine,* p. 1358. Society for Magnetic Resonance in Medicine, New York.

Morgan C. and Lazarow A. (1963) Immunoassay of insulin: two antibody system. *Diabetes* **12,** 115–126.

Mueckler M. (1994) Facilitative glucose transporters. *Eur. J. Biochem.* **219,** 713–725.

Neil J., Bosch C., and Ackerman J. (1994) An evaluation of the sensitivity of the intravoxel incoherent motion (IVIM) method of blood flow measurement to changes in cerebral blood flow. *Magn. Reson. Med.* **32,** 60–65.

Ordidge R. J., Connelly A., and Lohman J. A. B. (1986) Image-selected in vivo spectroscopy (ISIS). A new technique for spatially selective NMR spectroscopy. *J. Magn. Reson.* **66,** 283–294.

Pappenheimer J. and Setchell B. (1973) Cerebral glucose transport and oxygen consumption in sheep and rabbits. *J. Physiol. (Lond.)* **283,** 529–551.

Pardridge W. (1983) Brain metabolism: a perspective from the blood–brain barrier. *Physiol. Rev.* **63,** 1481–1535.

Petroff O., Spencer D., Alger J., and Prichard J. (1989) High-field proton magnetic resonance spectroscopy of human cerebrum obtained during surgery for epilepsy. *Neurology* **39,** 1197–1202.

Posse S., Cuenod C., Riesinger R., LeBihan D., and Balaban R. (1995) Anomalous transverse relaxation in ^{1}H spectroscopy in human brain at 4 Tesla. *Magn. Reson. Med.* **33,** 246–252.

Press W., Flannery B., Teukolsky S., and Vetterling W. (1989) *Numerical Recipes in Pascal.* Cambridge University Press, Cambridge.

Reivich M., Alavi A., Wolf A., Fowler J., Russell J., Arnett C., MacGregor R., Shiue C., Atkins H., Anand A., Dann R., and Greenberg J. (1985) Glucose metabolic rate kinetic model parameter determination in humans: the lumped constants and rate

constants for [^{18}F]fluorodeoxyglucose and [^{11}C]deoxyglucose. *J. Cereb. Blood Flow Metab.* **5,** 179–192.

Rothman D., Petroff O., Behar K., and Mattson R. (1993) Localized ^{1}H NMR measurements of GABA levels in human brain in vivo. *Proc. Natl. Acad. Sci. USA* **90,** 5662–5666.

Seaquist E. R., Pyzdrowski K., Moran A., Teuscher A. U., and Robertson R. P. (1994) Insulin-mediated and glucose-mediated glucose uptake following hemipancreatectomy in healthy human donors. *Diabetologia* **37,** 1036–1043.

Silver I. and Erecińska M. (1994) Extracellular glucose concentration in mammalian brain: continuous monitoring of changes during increased neuronal activity and upon limitation in oxygen supply during normo-, hypo- and hyperglycemic animals. *J. Neurosci.* **14,** 5068–5076.

Svarer C., Law I., Holm S., Morch N., Hasselbalch S., Hansen L., and Paulson O. (1996) An artificial neural network approach to estimation of the regional glucose metabolism using PET, in *Quantification of Brain Function Using PET* (Myers R., Cunningham V., Bailey D., and Jones T., eds), pp. 271–276. Academic Press, San Diego.

Taylor R., Price T., Rothman D., Shulman R., and Shulman G. (1992) Validation of ^{13}C NMR measurement of human skeletal muscle glycogen by direct biochemical assay of needle biopsy samples. *Magn. Reson. Med.* **27,** 13–20.

Whitesell R., Ward M., McCall A., Granner D., and May J. (1995) Coupled glucose transport and metabolism in cultured neuronal cells: determination of the rate-limiting step. *J. Cereb. Blood Flow Metab.* **15,** 814–826.

Willker W., Engelmann J., Brand A., and Leibfritz D. (1996) Metabolite identification in cell extracts and culture media by proton-detected 2D-H,C-NMR spectroscopy. *J. Magn. Reson. Anal.* **2,** 21–32.